

Stripes, Pseudogaps, and Van Hove Nesting in the Three-band tJ Model

R.S. Markiewicz

Physics Department and Barnett Institute, Northeastern U., Boston MA 02115

Slave boson calculations have been carried out in the three-band tJ model for the high- T_c cuprates, with the inclusion of coupling to oxygen breathing mode phonons. A generic phase separation is found, due to the competition of localization and magnetic effects near half filling. If the electron-doped regions can be suppressed, the phase separation would be between a hole-doped domain and a (magnetic) domain near half filling, with long-range Coulomb forces limiting the separation to a nanoscopic scale. Strong correlation effects pin the Fermi level *close to*, but not precisely at the Van Hove singularity (VHS), which can enhance the tendency to phase separation.

The resulting dispersions have been calculated, both in the uniform phases and in the phase separated regime. In the latter case, distinctly different dispersions are found for large, random domains and for regular (static) striped arrays, and a hypothetical form is presented for *dynamic* striped arrays. The doping dependence of the latter is found to provide an excellent description of photoemission and thermodynamic experiments on pseudogap formation in underdoped cuprates. In particular, the multiplicity of observed gaps is explained as a combination of two types of charge density wave (CDW) gaps plus a superconducting gap. The largest gap is associated with VHS nesting. The apparent smooth evolution of this gap with doping masks a crossover from CDW-like effects near optimum doping to magnetic effects (flux phase) near half filling. A crossover from large Fermi surface to hole pockets with increased underdoping is found. In the weakly overdoped regime, the CDW undergoes a quantum phase transition ($T_{CDW} \rightarrow 0$), which could be obscured by phase separation.

I. INTRODUCTION

The slave boson technique has frequently been applied to the study of strong correlation effects in metals^{1,2}. In the high- T_c cuprate superconductors, the intense theoretical activity now allows a detailed comparison of slave boson results with the results of quantum Monte Carlo (QMC) or exact diagonalization calculations. Qualitatively, the comparison is excellent: the latter calculations have confirmed slave boson predictions^{2–6} that (1) correlations preserve a Fermi-liquid-like energy dispersion, but renormalize the bandwidth ('flat bands')⁷; (2) a Mott transition to an insulating phase can only occur at exactly half filling, when the bare Cu-O energy splitting Δ_0 is larger than a critical value Δ_{0c} (compare Refs.^{8,9} and¹⁰). The agreement is semi-quantitative: the doping dependence of the chemical potential in the three-band

model is nearly the same when calculated by slave boson or by quantum Monte Carlo techniques^{11,12}, with a slightly smaller value of Δ_{0c} in the latter (Fig. 36 of Ref.¹³).

The usual slave boson technique does not incorporate the magnetic effects which are important near half filling. This may be phenomenologically remedied by including the lowest-order correction in $t^2/U \sim J$, producing a three-band tJ model^{14–16}. A finite J leads to a small reduction in Δ_{0c} , thereby improving agreement with QMC calculations. It has recently been demonstrated¹⁷ that the model provides a natural explanation for the occurrence of striped phases. The present paper utilizes the three-band tJ model to explore the role of Van Hove singularity (VHS) nesting in the cuprates. A clear crossover is found between a magnetic-dominated regime near half-filling and a charge-dominated regime near optimum doping. The model is found to give a good description of the observed pseudogap formation in these materials, as well as to explain why the charged stripes are pinned near the VHS.

II. SELF-CONSISTENT EQUATIONS

In a recent survey of the Van Hove scenario¹³, it was pointed out that there are actually two variants of the scenario, a *simple* and a *generalized* scenario. The simple scenario explores the role of a peak in the density of states (dos) on the normal state and superconducting properties, ignoring any possible role of competing instabilities. In the extended scenario, these competing instabilities – predominantly spin or charge density waves – play an essential role, which can lead to the suppression of the superconducting instability.

Prior slave boson calculations had shown that correlation effects (a large on-site Coulomb repulsion, U) tend to pin the Fermi level near the VHS over an extended doping range^{4,6,18}, and this has since been confirmed by a number of different techniques^{19–24}. It was suggested that nesting of the VHS's would lead to density wave instabilities which could successfully compete with superconductivity. This was modelled²⁵ in a one-band tight-binding model, where the pinning was approximated by adjusting the Fermi surface curvature such that the Fermi level was exactly at the VHS for all dopings. The resulting density wave-superconducting phase diagram is in good agreement with the experimentally observed pseudogap transition vs. doping²⁶.

Clearly, such a model is oversimplified. Strong correlation effects tend to suppress electron-phonon coupling

near half filling, suggesting that the density wave must cross over from spin-density-wavelike near half filling to charge-density wavelike near optimum doping. Whether such a crossover could be adequately described in a one-band model was not at all clear.

In the present paper, a self-consistent three-band tJ model calculation is presented for this crossover, confirming the main results of the simpler calculation, and suggesting a possible origin of striped phases in these materials.

The three-band tJ model Hamiltonian is the same as that presented in Ref.¹⁷, with the addition of a term due to the formation of a charge density wave (CDW) of breathing mode symmetry. No spin-dependent terms are included, so the present model does not describe either the Néel or the superconducting phases. Both the CDW and the magnetic flux phase, if present, break the symmetry of the even and odd Cu sites in a given layer, giving rise to a doubling of the unit cell area. In a basis set consisting of symmetric and antisymmetric combinations of the atoms on the two sublattices, the Hamiltonian matrix becomes

$$\begin{pmatrix} \Delta_+ & -2its_x & -2its_y & -i\Delta_m & -2tc_x\delta_b & -2tc_y\delta_b \\ 2its_x & 0 & u_0s_xs_y & -2its_x\delta_a & 0 & 0 \\ 2its_y & u_0s_xs_y & 0 & -2its_y\delta_a & 0 & 0 \\ i\Delta_m & 2its_x\delta_a & 2its_y\delta_a & \Delta_- & 2tc_x & 2tc_y \\ -2tc_x\delta_b & 0 & 0 & 2tc_x & 0 & u_0c_xc_y \\ -2tc_y\delta_b & 0 & 0 & 2tc_y & u_0c_xc_y & 0 \end{pmatrix} \quad (1)$$

where $\Delta_{\pm} = \Delta \pm \Delta_p$. In this matrix, the band parameters are Δ , the splitting between the Cu and O energy levels, $t_{CuO} = t(1 \pm \delta)$, the Cu-O hopping parameter, t_{OO} , the O-O hopping parameter, and Δ_1 a parameter associated with Cu-Cu exchange. In addition, $c_i = \cos(k_i a/2)$, $s_i = \sin(k_i a/2)$, $i = x, y$, and $u_0 = -4t_{OO}$.

δ is the asymmetry of the Cu-O hopping introduced by the CDW distortion; for a breathing mode, all four Cu-O bonds of one Cu are long ($t_{CuO} = t(1 - \delta)$), while all four bonds for the other Cu are short. There are two possible values for δ : let

$$\delta_k = \begin{cases} \delta_0 + \delta_1, & \text{if } |E'_k - E_F| \leq \hbar\omega_0; \\ \delta_0, & \text{otherwise,} \end{cases} \quad (2)$$

with ω_0 a phonon cutoff frequency and E'_k the quasiparticle energy in the absence of a CDW. The use of E'_k in Eq. 2 is a weak coupling approximation; it will be seen to lead to a slightly erroneous dispersion, in that the resulting gap is not exactly centered at E_F . In the Hamiltonian matrix, Eq. 1, the δ_i $i = a, b$ should be replaced by the appropriate δ_k , which may be different for the symmetric and antisymmetric Cu's.

At the mean-field level, magnetic exchange leads to an effective Cu-Cu hopping, of magnitude

$$\Delta_{ij} \equiv J \sum_{\sigma} \langle d_{i\sigma} d_{j\sigma}^{\dagger} \rangle = \Delta_1 e^{i\theta_{ij}}, \quad (3)$$

with i and j labelling adjacent Cu sites. A number of different magnetic phases are possible, depending on the choice of phase. Here only two magnetic phases are considered, the paramagnetic ($\theta_{ij} = 0$) and the flux ($\theta_{ij} = \pm\pi/4$)²⁷ phases. The paramagnetic phase is usually called the uniform phase, but here ‘uniform’ will be used in a different way, to denote the absence of a phase separation. In the flux phase, the \pm sign is chosen so that the net phase change around any plaquette is $\pm\pi$. For the paramagnetic phase, $\Delta_p = -2\Delta_1(\bar{c}_x + \bar{c}_y)$, $\Delta_m = 0$, with $\bar{c}_i = \cos k_i a$, $i = x, y$. For the flux phase, $\Delta_p = -\sqrt{2}\Delta_1(\bar{c}_x + \bar{c}_y)$ and $\Delta_m = -\sqrt{2}\Delta_1(\bar{c}_x - \bar{c}_y)$.

If the unrenormalized values of Δ and t are Δ_0 and t_0 respectively, then setting $r_0 = t/t_0$, the equations of self-consistency become

$$r_0^2 = \frac{1}{2} [1 - \frac{1}{N_s} \sum_k u_k^2 f_h(E_k)], \quad (4)$$

$$\Delta_0 - \Delta = \frac{1}{2r_0^2 N_s} \sum_k u_k^2 f_h(E_k)(E_k - \tilde{\Delta}), \quad (5)$$

and

$$\Delta_1 = \frac{J}{2N_s} \sum_k u_k^2 f_h(E_k) \gamma_{\vec{k}}, \quad (6)$$

where N_s is the number of unit cells E_k is the eigenvalue of H , $f_h(E_k)$ is the Fermi function, u_k is the amplitude of the wave function on Cu, and $\tilde{\Delta} = \Delta + 2\Delta_1\gamma_{\vec{k}}$. The function $\gamma_{\vec{k}} = \bar{c}_x + \bar{c}_y (\sqrt{\bar{c}_x^2 + \bar{c}_y^2})$ in the paramagnetic (flux) phase. As written, Eqs. 4 and 5 are valid for a hole picture, so $f_h(E_k) = 1$ for $E_k > E_F$, and = 0 otherwise (assuming $T = 0$). The Fermi energy is determined from

$$\frac{1}{N_s} \sum_k f_h(E_k) = 1 + x. \quad (7)$$

For the CDW, the additional self consistent equations are²⁸

$$\delta_0 = \frac{-V_{ep}}{2tN_s} \sum_k'' f_h(E_k) u_{1k}^* (v_{2x}c_x + v_{2y}c_y), \quad (8)$$

$$\delta_1 = \frac{-V_{ep}}{2tN_s} \sum_k f_h(E_k) u_{1k}^* (v_{2x}c_x + v_{2y}c_y), \quad (9)$$

where V_{ep} is the phonon-induced effective electron-electron interaction energy and the double prime on the first sum means that both $|E'_k - E_F| \leq \hbar\omega_0$ and

$|E'_{|\vec{k}+\vec{Q}|} - E_F| \leq \hbar\omega_0$, with $\vec{Q} = (\pi/a, \pi/a)$. Also, u_1 is the wave function amplitude for one (e.g., the symmetric) Cu, and v_{2x}, v_{2y} are the corresponding amplitudes for the (antisymmetric) oxygens.

In the present paper, the parameters are taken as $\Delta_0 = 6\text{eV}$, $t_0 = 1.3\text{eV}$, $t_{OO} = -0.45\text{eV}$, $J = 0.13\text{eV}$ and $\hbar\omega_0 = 50\text{meV}^{13}$. The free energy is

$$F = F_0 + \sum_k f_e(E_k) E_k, \quad (10)$$

$$F_0 = N_s \left[(\Delta_0 - \Delta)(1 - 2r_0^2) + \frac{2\Delta_1^2}{J} + \frac{t^2\delta_0\delta_1}{V_{ep}} \right]. \quad (11)$$

III. PHASE SEPARATION

A. Localization-Controlled Phase Separation

Figure 1 shows the doping dependence of the free energy for both the paramagnetic (solid line) and flux (dashed line) phases, in the absence of electron-phonon coupling¹⁷. Clearly, the phase at half filling is unstable against phase separation into hole-rich and electron-rich domains – the dotted line giving a tangent construction of the two equilibrium phases.

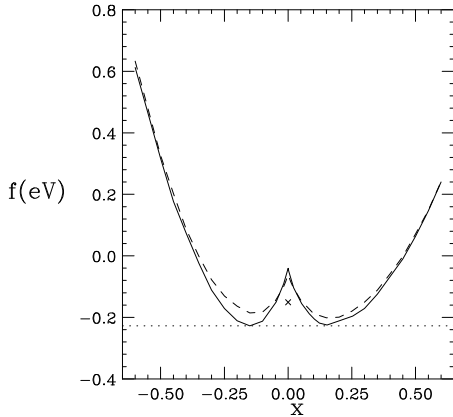


FIG. 1. Comparison of free energies in the paramagnetic (solid line) and flux (dashed line) phases. Dotted lines = tangent construction of coexisting phases. To accentuate the curvature in f , a term linear in x has been subtracted from all curves. The tJ model result at half filling is indicated by a \times .

There have been a number of theoretical suggestions that phase separation arises in a doped Mott insulator, some^{29,30} prior to the discovery of high- T_c superconductivity, and others^{31,32,4} in the specific context of the cuprates. However, detailed calculations have generally found that phase separation is either absent (in the pure Hubbard model^{33,34}) or is present only for unphysically

large choices of parameters, such as J (in the tJ model)³⁴, or the nearest neighbor Coulomb energy V (in the three-band extended Hubbard model)³⁵. By contrast, a phase separation is clearly indicated by a Maxwell construction based on plots of free energy vs. doping, both in the original tJ model^{36,37} and in the present three band tJ model¹⁷.

Some earlier studies attempted to find a divergence in the compressibility, which is difficult to identify numerically; other studies identified the chemical potential with the Fermi energy. However, when the band parameters have a strong doping dependence, this latter procedure is not justified, and the chemical potential must be found from $\mu = \partial F / \partial N_e$, where N_e is the number of electrons. The driving force for phase separation is a localization effect: when the Cu-O hopping $t \rightarrow 0$, the average kinetic energy of the electrons is raised¹⁷.

There is considerable experimental evidence for phase separation in the cuprates, which has been presented in a number of conferences³⁸ and reviews^{39,40,13}. However, whereas there is some evidence for a separation into electron-rich and hole-rich domains in the *electron*-doped $\text{Nd}_{2-x}\text{Ce}_x\text{CuO}_4$ (NCCO)^{41,42}, phase separation in the *hole*-doped cuprates has a very different character. Here, the phase separation is between a hole-doped phase and an antiferromagnetic insulator (AFI) phase close to half filling. The experimental evidence for this latter case falls into two categories, depending on whether the dopant ions are mobile or not. Thus, in $\text{La}_2\text{CuO}_{4+\delta}$, the doping is provided by interstitial oxygens⁴³ which are mobile below room temperature. When the holes bunch up, the interstitial O's follow, leading to a macroscopic phase separation between an undoped AFI and an optimally doped high- T_c superconductor. In other cuprates, the dopant ions are immobile, and the phase separation will be restricted to a nanoscopic scale due to Coulomb repulsion between holes. Tranquada and coworkers^{44,45} have demonstrated that in $\text{La}_{2-x-y}\text{Nd}_y\text{Sr}_x\text{CuO}_4$, when $x \sim 1/8$, commensurability effects pin the domains, allowing a clear observation of alternating charged and magnetic stripes. They suggest that similar stripes exist in other cuprates, but as dynamic fluctuations.

B. Electron-Hole Phase Separation

The phase separation exemplified by Fig. 1 is unique to the three-band model, and does not arise in the usual tJ model. In the tJ model, the limit of infinite on-site Coulomb repulsion is assumed, in that no site can be doubly occupied. Hence, only the upper or lower Hubbard band can be populated, and it is not possible for x to change sign. On the other hand, in the simplest three-band model, correlations are included only on the Cu atoms. Thus only the upper Hubbard band of the Cu can be partially hole occupied, but there is an additional, charge-transfer band associated with the O's. The insu-

lating gap arises between the Cu upper Hubbard band (for $x < 0$) and the O charge transfer band ($x > 0$). Since the gap between the two bands is finite, both may be partially occupied, leading to the novel phase separation of Fig. 1.

This phase separation raises an issue not contemplated in the usual theory of phase separation. That is the role of charge compensation when the holes and electrons start to bunch up. Consider first the uniform phases: hole doping requires a layer off of the CuO_2 planes which can act as an electron acceptor, while electron doping requires an electron donor layer. These layers will in general be very different chemically, leading to a discontinuous change in the doping as x passes through zero. Hence, uniform electron doping may well be impossible due to the properties of other layers in the cuprates.

This would also forbid an electron-hole nanoscale phase separation on the CuO_2 planes, if the average x is negative. However, what if the average x is positive? The nanoscale phase separation involves bunching of holes only on the CuO_2 planes, while the doping on the other planes may remain uniform. Hence, in principle the phase separation suggested by Fig. 1 is possible, as long as the average $x > 0$. How then would the Maxwell construction work? That would give only the average free energy of the holes, which would then have to be added to the free energy of the compensating charges. This could lead to a discontinuous behavior, where the electron-hole phase separation exists only up to half filling, but the system cannot be doped beyond.

The present paper is concerned with the question of the hole-doped cuprates, and hence I will suggest a plausible scenario in which the present free energy curves could be modified to eliminate the anomalous electron-rich domains. First, note that if the electron doped regime ($x < 0$) is simply assumed to be inaccessible, then the free energy curves of the flux and paramagnetic phases cross at a low doping, Fig. 1, leading to a weakly first-order phase transition, Fig. 2, between a flux phase near half filling ($x = x_1 \simeq 0$) and a paramagnetic hole doped phase at $x = x_c$. However, if the flux per plaquette is not restricted to the values zero and π (the phase θ_{ij} in Eq. 3 is allowed to vary continuously^{15,16}), then there can be a smooth crossover from the flux to the paramagnetic phase, without a discontinuous jump (see Ref.⁴⁶).

A stronger phase separation can be found if it is noted that the present slave boson calculation underestimates the free energy at half filling, due to neglect of Néel order. The importance of Néel-type (spin-dependent) terms can be directly demonstrated. Since $t \rightarrow 0$ at half filling, the oxygen bands decouple from the problem, and the free energy should be identical to that found in the one-band tJ model, and hence in the Hubbard model. This energy is known to be $E_H = -1.16934J$ ^{37,51}. As denoted by the \times in Fig. 1, this is lower than the slave boson result by a factor of ~ 2 . If the correct tJ value is assumed for the free energy at half filling, the width of the phase separated regime is greatly extended, as shown in Fig. 3.

Since the Néel transition decreases rapidly with doping, the free energy curves should change only for $x \leq 0.04$, so the Maxwell construction of Fig. 3 should be approximately correct. This is similar to the phase separation found in the tJ model^{36,37}. [Note that, depending on the exact dispersion, the free energy minimum may be shifted off of half filling.] The present picture of phase separation as a competition between magnetic order and delocalization is similar to that discussed by Nagaev³⁰.

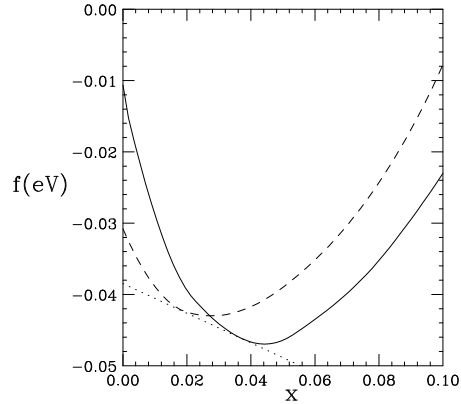


FIG. 2. Similar to Fig. 1, but assuming only $x > 0$ is allowed. Note that a different baseline has been chosen here.

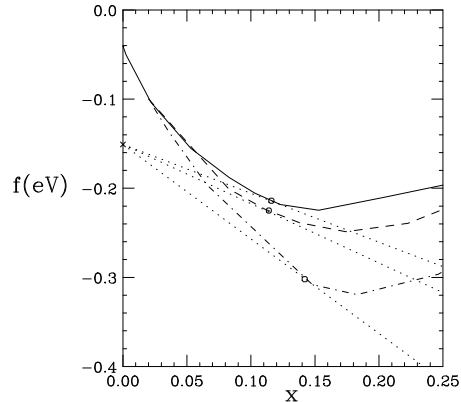


FIG. 3. Similar to Fig. 2, but using the one-band tJ model free energy at half filling. Solid curve = paramagnetic phase data of Fig. 1; dashed and dot-dashed curves correspond to finite values of V_{ep} , as in Fig. 6 below. Dotted lines indicate Maxwell constructions to the various curves, circles indicate hole doped end phases.

However, as shown in Fig. 1, the phase at half filling is still metastable with respect to the electron-hole phase separation. I suggest that the electron-doped phase is probably destabilized by interlayer strain effects, due to lattice constant mismatch between the CuO_2 layers and other layers in the crystal – e.g., the LaO layers in $\text{La}_{2-x}\text{Sr}_x\text{CuO}_4$ (LSCO)⁴⁷. These strains can be approximately written in the form¹⁷

$$f_{str} = \frac{K}{2}(x - x_0)^2. \quad (12)$$

As the doping passes through half filling ($x = 0$), the dominant chemical orbitals change, so the doping dependence of the equilibrium lattice constant can change its slope (e.g., see⁴⁸). This will mean that K can take on different values, K_{\pm} , depending on whether $x < 0$ or $x > 0$. Correspondingly, x_0 must change value, with $x_{0-}/x_{0+} = \sqrt{K_+/K_-}$ to ensure continuity of f . Figure 4 shows that, for suitable values of interlayer strain, it is possible to stabilize the Néel phase at half filling. There are other factors which can lower the free energy near half filling, such as a spin-Peierls phase^{49,50}. Still other possibilities are suggested in Ref.¹⁷. This issue will be taken up in future calculations.

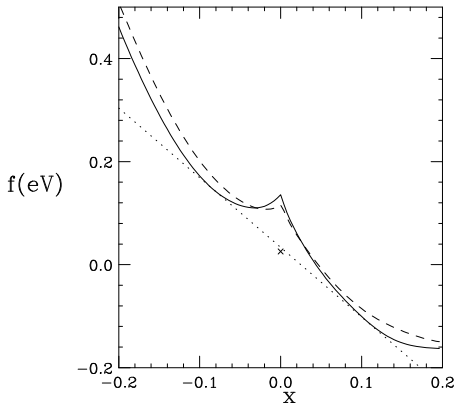


FIG. 4. Free energy curves similar to Fig. 1, but corrected for interlayer strain, Eq. 12, assuming $K_- = 8\text{eV}$, $K_+ = 2\text{eV}$, and $x_{0+} = 0.42$.

In the following, it will be assumed that the electron-doped regime has been eliminated, and that there is a phase separation between a flux phase with $x = x_1$ and a paramagnetic phase with $x_c \simeq 0.2$. The precise value of x_c is not important, but it will turn out to make a difference whether the flux phase is at $x_1 = 0$ or 0^+ . Before this phase separation is analyzed, the properties of the uniform phases will be briefly discussed.

IV. RESULTS: UNIFORM PHASES

A. CDW Gap

Whereas equations Eqs. 8 and 9 represent a BCS-like calculation of the CDW gap²⁸, the nature of the gap is very different from that found in a superconductor, since the pairing now involves an electron and a hole. From Equation 2, there are *two gaps* with very different properties. The term δ_0 produces a uniform gap throughout the Brillouin zone. This gap is *not* tied to the Fermi level, but has its own dispersion throughout the zone. However, it *is* tied to the VHS, and always splits the VHS density

of states (dos) peak into two components. On the other hand, the gap associated with δ_1 is localized near the Fermi level, but need not split the VHS degeneracy.

In the cuprates, it will be shown that the gaps near the VHS's tend to change the large Fermi surface into pockets near the $(\pi/2, \pi/2)$ points. Since the δ_1 gap only acts to enhance the δ_0 gap, the Fermi surface near these pockets remains ungapped, and hence available for, e.g., superconducting pairing.

These features are illustrated in Figure 5, for two different dopings with $V_{ep} = 1\text{eV}$. For both dopings, δ_0 leads to a similar splitting of the VHS degeneracy, but the δ_1 -associated gap is very different. For $x = 0.32$, the Fermi level is more than $\hbar\omega_0$ below the VHS, so there is a larger gap away from the VHS. For $x = 0.15$, the VHS is now within $\hbar\omega_0$ of the Fermi level, but now for both of the bands coupled by nesting (i.e., in Eq. 1, $\delta_a = \delta_b = \delta_0 + \delta_1$), so there are actually two δ_1 -type gaps near the VHS. Note that the gap associated with δ_1 is not exactly centered at E_F , and indeed has some dispersion of its own. This is due to the weak coupling Eq. 2, which measures the gap from the bands *in the absence of electron-phonon coupling*.

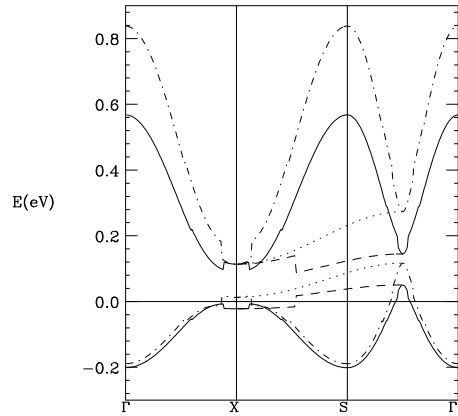


FIG. 5. Energy dispersion for the paramagnetic phase, for $V_{ep} = 1\text{eV}$, for $x = 0.15$ (solid lines) or 0.32 (dot-dashed lines). The dashed and dotted lines are the corresponding dispersions from X to $\tilde{S} = S/2$.

When Eq. 1 is Fourier transformed back to real space (and deconvolved from a symmetric/antisymmetric basis to an atomic basis), the term $\delta_a + \delta_b$ is found to correspond to a uniform breathing mode distortion, while $\delta_a - \delta_b$ produces an additional modulation with periodicity $\sim k_F^{-1}$, where \vec{k}_F is the wave number at the enhanced gap. This can be understood on the basis of simple hole counting: The uniform breathing mode distortion causes a doubling of the unit cell area. This can only produce a gap at exactly half filling (corresponding to a filled band in the supercell). To produce a gap at $x \neq 0$ requires a large superlattice, as would be produced by a commensurate value of \vec{k}_F .

These results clarify an issue that had been raised

earlier⁵². Whereas CDW effects have traditionally been associated with Fermi surface nesting, it was pointed out that polaronic band narrowing effects can be pinned to the VHS, and not the Fermi level, and hence can explain the observation of *extended* VHS's⁵³. Here we see that there are three related effects. The δ_0 gap is associated with the polaronic effects tied to the VHS, and will be seen to describe the photoemission observations of extended VHS's. In addition, there is an extra gap associated with δ_1 , when the quasiparticle energy is close to the Fermi level. Finally, this latter gap has a nesting enhancement when two pieces of Fermi surface are separated by the nesting vector (here, $Q = (\pi/a, \pi/a)$). From Eq. 9, only in the latter case does the gap contribute to the self-consistent equation for δ_1 .

B. VHS Pinning

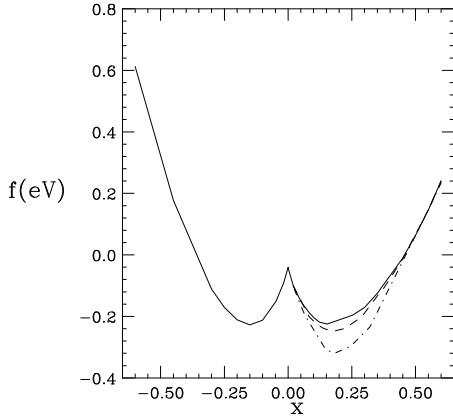


FIG. 6. Free energy $f = F/N_s$ in the paramagnetic phase as a function of hole doping x , for several values of electron phonon coupling, $V_{ep} = 0$ (solid line), 0.6eV (dashed line), or 1eV (dotdashed line). A term linear in x has been subtracted from all curves.

Figures 6 and 3 show the free energy $f = F/N_s$ for the paramagnetic phase for three values of $V_{ep} = 0, 0.6$, or 1eV. The instability of the phase near half filling, found in the absence of electron-phonon coupling, is found to be enhanced for $V_{ep} \neq 0$. It can be seen that the free energy lowering due to the CDW has a strong x -dependence: the free energy lowering vanishes as $x \rightarrow 0$ and is absent for electron doping. It also vanishes for too large hole doping. This result is due to VHS nesting: the strongest CDW effects occur when the Fermi level is close to the VHS. Note that, since the *shape* of the Fermi surface is doping dependent, the VHS remains pinned close to the Fermi level over an extended doping range. Nevertheless, the free energy lowering has a well defined maximum. This is better seen in Fig. 7, which plots the difference in free energy between the calculations for finite V_{ep} and those with $V_{ep} = 0$. This free energy lowering is approximately

quadratic in V_{ep} . The free energy lowering is roughly proportional to the magnitude of the CDW gap, Δ_{DW} , Fig. 8.

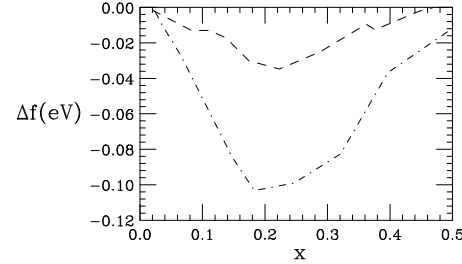


FIG. 7. Free energy difference $\Delta f = f(V_{ep}) - f(0)$ for the paramagnetic phase with $V_{ep} = 0.6$ eV (dashed line) and 1.0eV (dotdashed line).

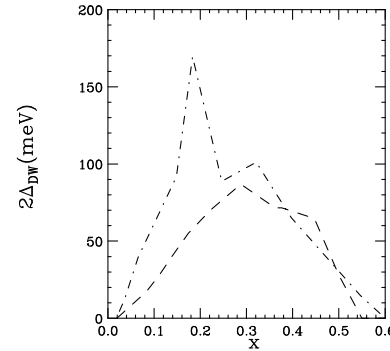


FIG. 8. CDW gap $2\Delta_{DW}$ plotted vs doping in the paramagnetic phase for $V_{ep} = 0.6$ eV (dashed line), or 1eV (dot-dashed line).

These electron-phonon effects are found to be absent in the flux phase. This is because the flux phase itself has already taken advantage of VHS nesting to lower its free energy, as can be seen in Fig. 9.

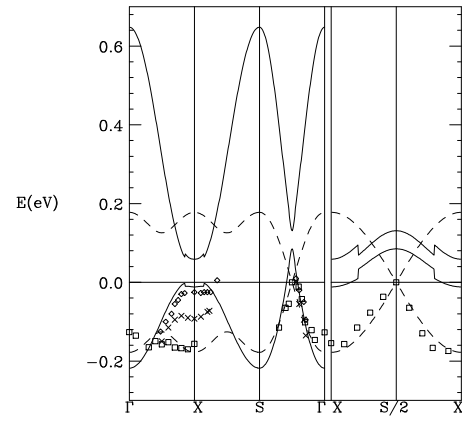


FIG. 9. Energy dispersion for the flux phase at half filling $x_1 = 0^+$ (solid line) and the paramagnetic phase at $x = 0.22$, $V_{ep} = 0.6\text{eV}$ (dashed line), close to the minimum of Δf . Data from underdoped Bi-2212 (diamonds and \times 's)⁵⁴ or SCOC (squares)⁵⁵ are plotted as $E/2$. Special points of the Brillouin zone are $X = (\pi, 0)$, $S = (\pi, \pi)$.

These results confirm and quantify the prediction⁴ that electron-phonon coupling near the VHS leads to a free energy minimum, which can by itself lead to a phase separation. In the present instance, the homogeneous paramagnetic phase is already unstable, but the nesting effect tends to pin one of the two phases close to the VHS. This is illustrated in Fig. 3, which shows that with increasing V_{ep} , the hole doped end phase of the phase separation regime moves toward higher doping, closer to the doping of minimum Δf . Figure 10 plots the energy difference between the VHS and the Fermi level. In the absence of electron-phonon coupling (solid line), the Fermi level crosses the VHS twice, at $x = 0$ and $x = \tilde{x}_c$, and correlation effects pin the Fermi level close to the VHS for $0 \leq x \leq \tilde{x}_c$. However, for the large assumed value $t_{OO} = -0.45\text{eV}$, \tilde{x}_c is small, leading to pinning in a narrow range of doping only. In the presence of a CDW, the energy bands split near the X -point of the Brillouin zone, Fig. 9, with each X -point band edge forming a separate VHS dos peak. The Fermi level is now even further from the average position of the VHS, taken as the middle of the X -point gap. However, the *lower VHS peak is found to be pinned about 10-20meV below the Fermi level over a wide range of dopings*, Fig. 10. This is in striking agreement with photoemission observations of optimally doped cuprates. Due to this strong pinning effect, it is difficult to define just what doping corresponds to the VHS. However, the hole-doped end phase of the phase separation regime will almost certainly be found to be pinned near a VHS.

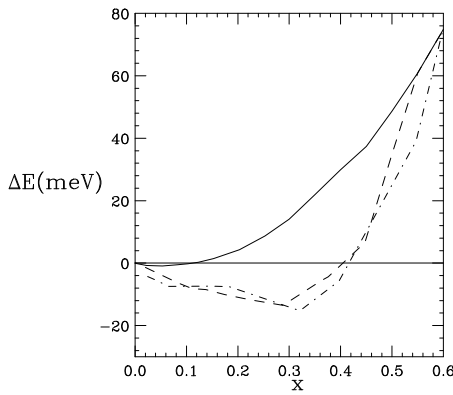


FIG. 10. Energy separation between the VHS and the Fermi level $\Delta E = E_{VHS} - E_F$, in the paramagnetic phase for $V_{ep} = 0$ (solid line), 0.6eV (dashed lines), or 1eV (dot-dashed lines). For $V_{ep} \neq 0$, the VHS is split; the present lines refer to the lower VHS's. For the $V_{ep} = 1\text{eV}$ data, the extra splitting due to δ_1 is neglected.

While there is no evidence for long-range CDW order in the cuprates, there is considerable evidence for short-range lattice disorder, summarized in Ref.¹³, Section IXB. While a substantial part of this local order is associated with tilting the CuO_6 octahedra out of the planes, there is also a significant contribution associated with CuO bond stretching⁵². Considerable work will be required to sort out the relative contributions of various phonon modes. For now, the breathing mode CDW is chosen to approximately represent the free energy lowering associated with this short-range order.

C. Insulating Regime

At half filling, for $\Delta_0 > \Delta_{0c}$, there is an insulating phase with $r_0 = 0$, but $\Delta_1 \neq 0$, with energy dispersion

$$E = \Delta + 2\Delta_1\gamma_{\vec{k}}. \quad (13)$$

At this doping, the free energy has a cusp (Fig. 6), so the chemical potential has a discontinuity: Δ in Eq. 13 takes on different values depending on whether $x = 0$ is approached from positive or from negative values. These two states have the same free energy, even though their effective Fermi levels differ by the charge transfer gap. Here is a clear case where the Fermi level does not coincide with the chemical potential, which is pinned in the middle of the gap. Thus photoemission should see a band with finite dispersion, Eq. 13, separated from the chemical potential by half the charge transfer gap.

Note that this band is only half full, but because of strong correlation effects the remaining states are no longer accessible. This is reminiscent of the upper and lower Hubbard bands, although these are now charge-transfer bands. This splitting of the band is readily done in the flux phase, since the lower and upper halves of the band are only connected at a few isolated points (diabolical points). However, it creates topological problems for the paramagnetic phase. Since the Fermi surface in the paramagnetic phase is square (at exactly half filling, Eq. 13), these problems can easily be overcome by opening a gap at the Fermi level – either due to antiferromagnetism or to a period doubling charge density wave. Note that this strongly suggests that the opening of a correlation gap must be accompanied by some other kind of ordering.

The split-off charge transfer band may have been observed experimentally⁵⁵. Since $t \rightarrow 0$, the dispersion is independent of all hopping parameters (e.g., t_{OO}). Hence, in the absence of longer-range exchange terms, the dispersion should be characteristic solely of the type of magnetic order, and should be the same as in the one band tJ model. Thus, it is interesting to note that the dispersion in the paramagnetic phase matches that calculated in the tJ model^{56,57}, while the flux phase dispersion matches that found in insulating $\text{Sr}_2\text{CuO}_2\text{Cl}_2$ (SCOC)⁵⁵, Fig. 9. This has also been noted by Laughlin⁵⁸ and Wen and Lee⁵⁹.

The magnitude of the predicted bandwidth can also be estimated. Using the mean field decoupling, the equilibrium value of Δ_1 in the paramagnetic phase is $4J/\pi^2 = 0.406J$, which is comparable to that found in Ref.⁵⁶, $\Delta_1 \simeq 0.55J$. In the flux phase, $\Delta_1 = 0.479J$, so $f = -2\Delta_1^2/J = -0.459J$, considerably smaller than the one band tJ result, $E_H = -1.16934J$. As discussed above, this is presumably due to neglecting the Néel order, and will be addressed in a future publication. Δ_1 monotonically decreases in magnitude as the system is doped away from half filling (in agreement with four-slave-boson calculations⁶⁰).

V. PSEUDOGAPS IN THE UNDERDOPED REGIME

A. The Experimental Situation

Above, it was shown that the CDW gap is expected to have two components, one tied to the VHS and one to the Fermi surface. In a similar fashion, photoemission studies in underdoped $\text{Bi}_2\text{Sr}_2\text{CaCu}_2\text{O}_8$ (Bi-2212) find two gap-like features, one tied to the Fermi level, and the other much larger gap near the VHS. The former gap is a d-wave like gap, with a maximum value of 25meV near $(\pi, 0)$ and a minimum value of ~ 0 near $(\pi/2, \pi/2)$ ^{61,62}. The gap magnitude is nearly independent of doping, but it opens up at the pseudogap temperature – i.e., at the superconducting transition in optimally doped material, but at a higher temperature in underdoped samples. This gap thus has some features of the Fermi surface CDW gap discussed above, but combined with the superconducting gap. In this paper, more attention will be placed on the second, VHS-related gap.

In the underdoped regime, the photoemission studies find a peak near the X point, which shifts further below the Fermi level with increasing underdoping⁵⁴, Fig. 9. The Stanford group⁵⁴ reports a continuous evolution of this peak with underdoping, approaching a dispersion near half filling similar to that found in the insulating compound SCOC⁵⁵, squares in Fig. 9.

On the other hand, Campuzano⁶³ proposes a different doping dependence of this feature. He suggests that there are two independent features near $(\pi, 0)$ in the Brillouin zone, one a sharp quasiparticle peak which is near the Fermi level at optimum doping, and broadens severely in underdoped samples, and the second a broad peak which is already present at ~ 200 meV below the Fermi level in optimally doped material, and gradually shifts to 300meV with increased underdoping. While additional experimentation is necessary to see which interpretation of the data is correct, it should be noted that either version can be understood within the present model. It will turn out that the data can only be understood as a dynamic average of the two separated phases represented by the solid and dashed lines in Fig. 9. If the fluctua-

tions are fast compared to the experimental observation technique, the data will give an average dispersion which evolves smoothly with doping, as in the Stanford interpretation. A quasistatic fluctuation, on the other hand, would produce results closer to Campuzano, with one peak gradually disappearing as the other peak grows up with underdoping.

Thermodynamic measurements of the pseudogap by Loram, et al.^{64,65} in underdoped $\text{YBa}_2\text{Cu}_3\text{O}_{6+y}$ (YBCO) and LSCO are in better agreement with the Stanford photoemission data⁵⁴. They have measured the dos from susceptibility and heat capacity measurements and find that a pseudogap appears and grows with successive underdoping. At $y = 0.3$ in YBCO, the peak of the gap is at $\Delta_g \simeq 100$ meV, comparable to the larger photoemission gap seen in Bi-2212. The gap can be fit to a d-wave gap – i.e., a logarithmic divergence at $E = E_F + \Delta_g$, as at a VHS, but with the dos $\rightarrow 0$ at $E \rightarrow E_F$. Presumably, these measurements are seeing a superposition of the two gaps seen in photoemission.

There are also photoemission data on underdoped YBCO^{66,67}, but they do not reveal a similar gap opening. Since the effects are rather subtle, perhaps additional measurements are needed.

B. Pseudogaps in the Uniform Phases

Figure 9 compares the dispersion observed for a series of underdoped samples of $\text{Bi}_2\text{Sr}_2\text{Ca}_{1-x}\text{Dy}_x\text{CuO}_8$ with the theoretical dispersions from the two equilibrium phases at $x = 0^+$ and $x = x_c$. While the theoretical calculations match the optimally doped and extremely underdoped limits, the agreement breaks down at intermediate dopings. Figure 8 shows that the density wave gap decreases with decreasing x , while the experimental gap increases. The problem with the theory is that the two gaps have independent origins – a CDW or a flux phase – and do not evolve smoothly into one another. In the following section, it will be shown that dynamic phase separation allows a smooth evolution between the two limits.

VI. CALCULATIONS FOR STRIPED PHASES

In the presence of phase separation, the dispersion will change. For a macroscopic phase separation, the photoemission would be a superposition of the two coexisting phases. However, in the present case, the phase separation is due to the holes only, so due to strong Coulomb effects (charging of the domains), the ensuing phase separation is on a nanoscopic scale only, which should lead to a more complex dispersion. There is evidence that in the cuprates, the phase separation is manifested in the form of alternating charge and magnetic stripes^{44,45}, with a well defined periodicity that varies smoothly with

doping. For any commensurate periodicity, the dispersion will have additional minigaps associated with the superlattice periodicity⁶⁸. Since the stripes are generally dynamic, these superlattice gaps will probably be washed out.

A proper calculation of the self-consistent, dynamic stripe phases is beyond the scope of the current paper. Instead, I will suggest a number of plausible forms for the average dispersion, and show that it is possible to explain the observed photoemission data. There is considerable flexibility in the results, and it appears likely that different dispersions can be observed, depending on the spacing of the stripes, and on whether the stripes are effectively static or dynamic (i.e, on the time scale of the observational technique).

A. Large Stripes

To simplify the problem, it is assumed that the fluctuations lead to a disorder in which any local region could have either of the two dispersions at random. The average dispersion can then be calculated by a CPA (coherent phase approximation) calculation^{69,68}. Repeating the calculation of Ref.⁶⁸, but assuming a random mix of only two phases, with Green's functions G_1 and G_2 and probabilities p_1 and $p_2 = 1 - p_1$, the average Green's function is (exactly) given by

$$G_0 = p_1 G_1 + p_2 G_2. \quad (14)$$

(Note that the assumption that the domains are large enough to have well defined G_1, G_2 is an implicit assumption of macroscopic phase separation.) Since the dispersion is given by real solutions of $G_0^{-1} = 0$, the photoemission dispersion should simply be a weighted superposition of the dispersions of the two end phases, with $G_1^{-1} = 0$ or $G_2^{-1} = 0$. (The latter correspond to the eigenvalues of the Hamiltonian, Eq. 1, in the two coexisting phases.) A similar solution was found in Refs.^{70,13}.

Here, the distinction between the flux phase being at $x = 0$ or 0^+ can be readily understood. At $x = 0$, the Fermi level lies in the middle of the charge transfer gap. Hence, the doping dependence predicted by Eq. 14 implies a gapped state at half filling, which persists in the doped material, with the appearance of midgap states in the doped material, with intensity increasing linearly with x . This is the form discussed in Refs.^{70,13}, and seems to provide a good description of photoemission experiments in a number of three-dimensional d-electron systems⁷¹. It would also be consistent with the photoemission data on underdoped YBCO⁶⁶, although it is not clear why these data are inconsistent with the heat capacity results⁶⁴.

However, this does not provide a good description of the photoemission data in Bi-2212, Fig. 9. A simple modification of the theory can significantly improve the agreement. If the phase separation starts not at $x = 0$,

but at a small positive doping $x_1 = 0^+$, then the doping dependence of the photoemission would be as follows. For doping between $x = 0$ and x_1 , there is no phase separation. The system remains in the flux phase, with the Fermi level again at midgap in undoped material, but shifting immediately to the top of the lower charge transfer band as soon as the first holes are doped in. This state is in good agreement with the experimental data on the most underdoped Bi-2212 samples, Fig. 9. With increased doping, the two phase regime is reached. (Note that in this doped regime, the optical conductivity can still see a charge transfer gap².)

The present model would predict a superposition of the two end phases, rather similar to Campuzano's interpretation of the data, but not consistent with the continuous evolution of the pseudogap suggested by the Stanford⁵⁴ and Loram^{64,65} results. This lack of agreement is not surprising. Such a macroscopic phase separation would also predict a unique value of the superconducting transition temperature T_c (the flux phase at x_1 being nonsuperconducting). The experimental observation that T_c evolves smoothly with doping strongly suggests that the phase separation is on such a nanoscopic scale that T_c evolves with doping via a form of proximity effect between the two phases. This same effect should explain the observed behavior of the pseudogap.

On a deeper level, the striped phases constitute a new thermodynamic state of matter, which can have a doping dependent T_c . A good analogy is provided by a superconductor in a magnetic field. In a type I superconductor, there is a macroscopic phase separation between domains wherein the magnetic field is non zero, quenching the superconductivity, and superconducting domains with zero field. Increasing the field reduces the fraction of the material which is superconducting, but T_c does not change with field. In a type II superconductor, the field domains are shrunk down to nanoscopic size as magnetic vortices, producing a novel state of matter in which T_c is a continuously varying function of the field. In the following subsections, a model is provided for the pseudogap in the striped phases.

B. Small Static Stripes

If the stripe pattern is static and commensurate with the crystalline lattice, then the stripes will provide a superlattice to modify the dispersion of the separate phases. Since the resulting dispersion is profoundly modified, it would be appropriate to repeat the self-consistent calculations in the presence of the stripes. Without attempting this difficult procedure, however, a qualitative understanding of the results can be achieved by using the self-consistent band parameters calculated for the two phases in equilibrium, at $x = x_1 > 0$ and $x = x_c$. For definiteness, the end phases are assumed to be the flux phase at $x_1 = 0^+$ and the paramagnetic phase with $V_{ep} = 0.6\text{eV}$,

$$x_c = 0.288.$$

Specifically, the stripes are assumed to be uniform along the y direction, and of periodicity $m+n$ Cu atoms along x , with m Cu atoms in the magnetic phase and n Cu's in the charged phase ($x = x_c$). For the cuprates, the x and y axes run parallel to the Cu-O-Cu bonds. All of the band parameters can be assigned values corresponding to either the flux phase at x_1 or the paramagnetic phase at x_c , except for the magnetic coupling of a Cu atom in the magnetic phase with a neighboring Cu in the charged phase. For these atoms, Δ_1 is taken as the average of the magnitudes of the Δ_1 's in the two phases, with zero phase factor. With these assumptions, the dispersion is a unique function of m and n . Figures 11 ($m = n = 2$) and 12 ($m = 2, n = 6$) provide representative illustrations of the complicated dispersion to be expected. There are $2(m+n)$ subbands, with very small dispersion along the x direction, since $t \simeq 0$ in the flux phase. Note that, because of this small dispersion along X , the dispersion along $\Gamma \rightarrow Y$ is nearly the same as that along $X \rightarrow S$.

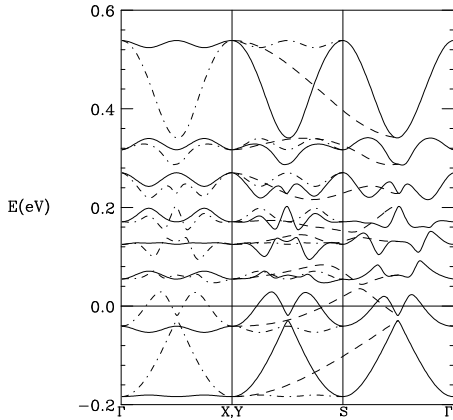


FIG. 11. Energy dispersion for a static striped phase, with $n = 2$ charge layers and $m = 2$ magnetic layers. Solid line (dotdashed line): dispersion along $\Gamma \rightarrow X(Y) \rightarrow S$; dashed line: dispersion along $X \rightarrow S/2$.

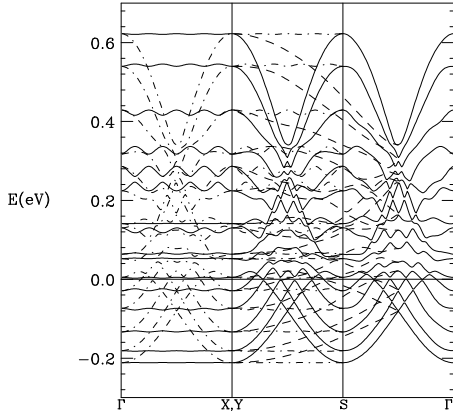


FIG. 12. Energy dispersion for a static striped phase, as for Fig. 11, but with $n = 6$ charge layers and $m = 2$ magnetic layers.

Once again, the results do not greatly resemble the photoemission data. Presumably, this is because the domains are fluctuating dynamically. If photoemission from a static domain pattern could be observed, then the minigaps predicted here should be observed if the domains are nearly commensurate and disorder effects are small. In particular, the dispersion of Fig. 11 has a hole doping $x_c/2 = 0.144$, and should be similar to the $x = 1/8$ phase of LSCO and $\text{La}_{2-x}\text{Ba}_x\text{CuO}_4$. [Note that the experiments of Tranquada, et al.⁴⁴ determined the overall periodicity of the stripes, but only *assumed*, on analogy with the nickelates, that the charge stripes were one cell wide, corresponding to a hole doping $x = 0.5$. An equally good case can be made¹³ for the assumption that the charge stripes are two cells wide, with $x \simeq 0.25$. This is consistent with the results of White and Scalapino⁷².]

The stripe pattern should be essentially static on the time scale of an optical absorption. Thus, the large number of very flat bands along $\Gamma \rightarrow X$ suggest that there should be a strong optical absorption associated with intersubband transitions. In the low doping limit, there may be a characteristic series of absorptions associated with an isolated charge stripe, but in the higher doping regime, peaks from several different stripe configurations should overlap to produce a more-or-less continuous band between ~ 0 - 0.8 eV. This is fairly close to the mid-infrared band found in most of the cuprates, with a broad peak near 0.4 eV.

C. Dynamic Stripes

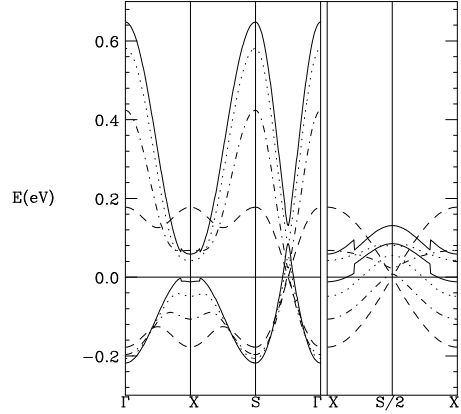


FIG. 13. Energy dispersion for the fluctuating stripe phase model, for $\nu_c = 0$ (dashed line), 0.5 (dotdashed line), 0.75 (dotted line), and 1 (solid line).

Notice that once nanoscopic stripes are formed, the averaging inherent in Eq. 14 is lost: no domain is large

enough to have the dispersion characteristic of G_1 . Now the band parameters have become local functions of space and, in dynamic stripes, of time as well. This can best be thought of as a generalization of the zero sound modes of a Landau Fermi liquid – shape oscillations of the Fermi surface due to electron-electron interaction. I propose that in this state, when the stripe motion is rapid enough that only average properties are apparent, the appropriate procedure (replacing Eq. 14) is to *average the band parameters themselves*.

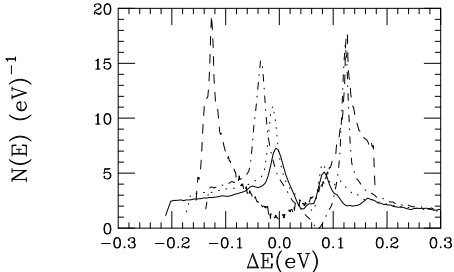


FIG. 14. Density of states vs. energy $\Delta E = E - E_F$ for the fluctuating stripe phase model, for $\nu_c = 0$ (dashed line), 0.5 (dotdashed line), 0.75 (dotted line), and 1 (solid line).

This is done in Fig. 13, for several intermediate dopings. The resulting dispersions are in good agreement with the experimental data, Fig. 9. The photoemission studies find that at optimum doping, the Fermi level is close to an *extended* VHS, which evolves into a bifurcated VHS in underdoped Bi-2212 (for a bifurcated VHS, the dispersion has two minima offset from the X point along the $\Gamma - X$ line of the Brillouin zone). These results are well reproduced in the present calculations.

Figure 14 shows the calculated densities of states, illustrating the splitting of the VHS degeneracy. Note that in the unmodulated phase at $x = x_c = 0.288$, the VHS is split, but there is no true gap (with $N(E) = 0$). This is because the δ_0 gap has a dispersion, so parts of the Fermi surface remain ungapped, at least in the absence of superconductivity. For lower doping, the effective Fermi surface becomes closer to a square, and there is a gap over the full Fermi surface.

The opening of the pseudogap with underdoping found in Fig. 14 is in good qualitative agreement with the heat capacity measurements of Loram, et al.^{64,65}. They have fit the dos lineshape to a d-wave gap, and Figure 15 shows that the dos calculated for $\nu_c = 0.5$ does indeed bear a strong resemblance to a d-wave gap (dashed line).

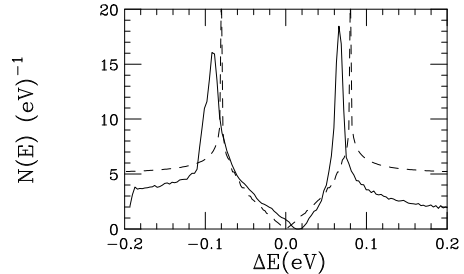


FIG. 15. Density of states vs. energy $\Delta E = E - E_F$ for the fluctuating stripe phase model, for $\nu_c = 0.5$ (solid line), compared to the calculated dos for a d-wave gap (dashed line).

A closer comparison of the data, Fig. 9, and the theory, Fig. 13, reveals excellent agreement near Γ (e.g., along $\Gamma \rightarrow X$), but an absence of the experimental points near $S = (\pi, \pi)$ (e.g., along $X \rightarrow S$). This is the ‘ghost’ part of the dispersion, and it is found to be weak even in the limiting case of SCOC (squares in Fig. 9). The evolution of the Fermi surface with doping shows a clear crossover from a large Fermi surface, Fig. 16, to a small Fermi surface, Fig. 17. Once again, the shapes of the Fermi surfaces are in good agreement with photoemission, except in the ghost part of the dispersion. Note also that at the highest doping, $x = 0.288$ (Fig. 16), the Fermi surface is approximately a circle centered on the point (π, π) (accompanied by its ghost near Γ). This is the form of Fermi surface assumed in the tJ model in Ref.³⁷, and the breakdown of this assumption for lower doping explains why their calculation is restricted to $x \geq 0.3$.

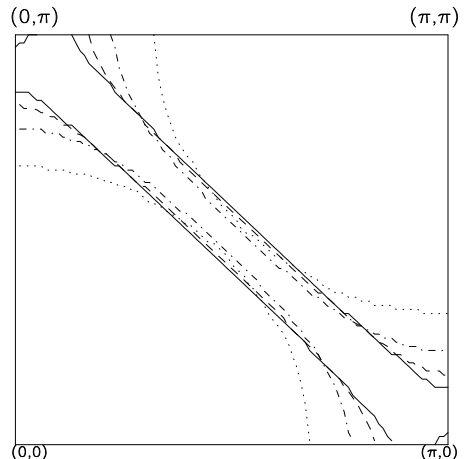


FIG. 16. Fermi surfaces for the fluctuating stripe phase model, for $\nu_c = 1.0$ (dotted line), 0.625 (dotdashed line), 0.5625 (dashed line), and 0.5486 (solid line).

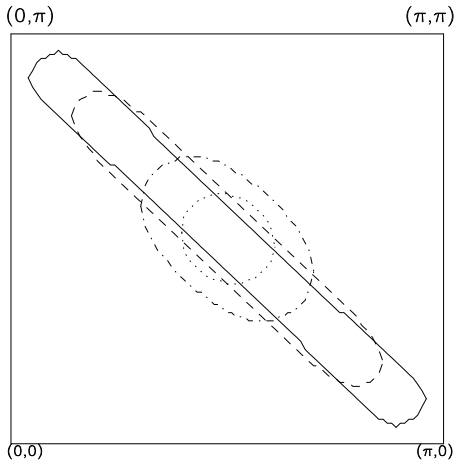


FIG. 17. Fermi surfaces for the fluctuating stripe phase model, for $\nu_c = 0.125$ (dotted line), 0.25 (dotdashed line), 0.5 (dashed line), and 0.5469 (solid line).

Note that while the theoretical data in Figs. 1-9 are based on the self-consistent slave boson calculations of the flux and paramagnetic phases or on the result of a more exact calculation^{37,51} (the point marked \times in Figs. 1 and 3), the results of this section, Figs. 13-17, require one additional assumption. This is the assumption that, in the presence of a dynamic stripe phase, the proper average over these stripes is given by the weighted average of the band parameters of the two coexisting phases.

VII. DISCUSSION

The above calculations have provided a plausible explanation for the opening of a double pseudogap in underdoped Bi-2212, while providing a sounder underpinning for the earlier one-band calculations of Ref.²⁵. The present results are in excellent agreement with these earlier calculations, which can therefore be used to supplement the present T=0 calculations. Here, the detailed correspondence between experiment and theory will be briefly summarized, including calculations of superconducting properties and temperature dependences from the one-band model.

First and foremost, it should be noted that Fig. 14 is a very clear demonstration that the physics of the underdoped cuprates is dominated by VHS nesting. Secondly, the model is not merely consistent with the underlying presence of striped phases (or similar manifestations of nanoscale phase separation), it *requires* them to reproduce the smooth doping dependence of the pseudogap magnitude. Thirdly, it correctly reproduces the characteristic double gap structure which has been such a puzzling feature of the photoemission experiments: the large splitting of the VHS degeneracy, associated with δ_0 , and the smaller pulling back of dos from the Fermi level, associated with δ_1 . Since both are aspects of a

single transition, both disappear at the same pseudogap transition temperature, as found experimentally.

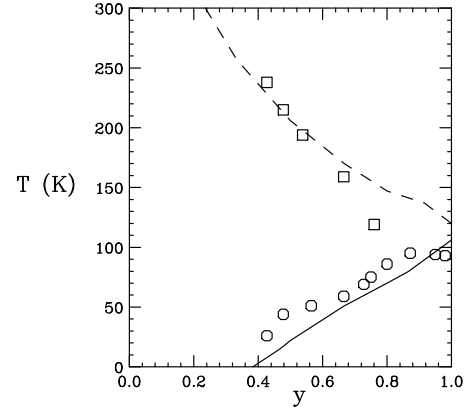


FIG. 18. Phase diagram of the pseudogap (dashed line) and superconducting (solid line) phases, based on the one-band model, and compared to the experimental data of Loram, et al.⁷³ for $\text{YBa}_2\text{Cu}_3\text{O}_{6+y}$.

Figure 18²⁶ shows that the model reproduces the experimentally observed⁷³ pseudogap phase diagram, including a doping dependent superconducting T_c . The competition between pseudogap and superconductivity displayed in Fig. 18 can be understood in terms of the evolution of the shape of the Fermi surface with doping. The VHS is pinned by correlation and phase separation effects near the Fermi surface; this pinning means that the shape of the Fermi surface must evolve with doping, being square at half filling, and curved in such a way as to accommodate more holes as doping increases. Since the pseudogap is associated with nesting, it dominates near half filling, when the nesting is perfect. Away from half filling, the nesting is worse, so the pseudogap and pseudogap transition temperature both rapidly decrease with doping. Superconductivity requires a large dos, but is insensitive to nesting; moreover, it can arise on those sections of Fermi surface which survive the imperfect nesting. For both of these reasons, the superconducting transition temperature grows with increasing doping, until it is comparable to the density wave transition.

Within the model, the pseudogap arises from a structural or magnetic instability – actually, there is a crossover between the two effects with increased underdoping. Neither has any direct relation with superconductivity, except that they compete with it for the large dos associated with the VHS. Superconductivity first arises in the model from the leftover dos associated with parts of the Fermi surface away from the VHS. This is illustrated in the one-band model calculation of Fig. 19. The solid lines in this figure should be compared to the dotted lines in Fig. 13. The main difference is the superconducting gap away from the VHS – near the hole pockets at $S/2$, although there is a weak superconducting contribution to the gap at the VHS. Thus, unlike Fig.

14, in the presence of a superconducting gap, the dos will vanish at the Fermi level.

This extra gap helps to explain the smaller photoemission gap, which has d-wave symmetry, vanishing near $S/2$. Without superconductivity, the density wave gaps would vanish in a finite portion of the Brillouin zone near $S/2$. Thus, the fact that the gap remains finite except exactly at $S/2$ is probably due to (d-wave) superconductivity. The doping dependence of the gap near X, Y , is unexpected for the present model, which would predict roughly a scaling of the superconducting gap with ν_c^{25} . Instead, it is found that the *gap* increases weakly with increased underdoping⁷⁴, while the *temperature* at which the gap opens increases more rapidly, proportional to the large pseudogap. This suggests that the X, Y gap is associated with the CDW. Even here, to replicate this behavior would require a finite value of δ_1 in the flux phase at x_1 . However, this cannot be associated with the oxygen breathing mode discussed above, since correlation effects renormalize it to zero at half filling. There could, however, be a finite spin-Peierls distortion of the Cu ions^{49,50}.

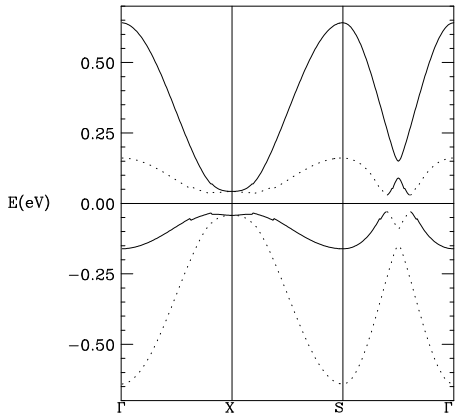


FIG. 19. Energy dispersion in the one-band model, in the presence of superconductivity. Dotted lines = hole-like part of dispersion (electron-like part reflected around Fermi level). Only the electron-like part (solid lines) will be visible in, e.g., a photoemission experiment. To stress the role of the superconducting gap, the smaller CDW gap, δ_1 , has been set equal to zero.

One important prediction of the model is thus that there is *yet another gap*, specifically associated with the superconducting transition, which increases with increasing hole doping, scaling with the superconducting T_c . Evidence for such a gap is found in neutron scattering measurements of the magnetic susceptibility near $S = (\pi, \pi)$, which see a spin gap followed by a resonance peak, both of which features scale with T_c^{75} . Such a spin gap follows from BCS theory. To be consistent with Fig. 19, the susceptibility must be associated with scattering between sections of Fermi surface near $S/2$ which are not gapped by the density wave order.

Within the present model, the issue of *overdoping* can be briefly addressed. From the free energy curves of Fig. 1, it appears that the system will continue to evolve in a uniform paramagnetic phase for doping beyond the phase separated regime. However, the free energy has a local minimum near optimal doping, which is likely to be enhanced by the difficulty of adding additional holes to the CuO₂ planes. Hence, there may well be another phase with lower free energy, probably associated with doping holes off of the planes (perhaps onto the apical O's and Cu-d_{z2}'s) in this doping range. The crossover from the optimally doped phase to this overdoped phase will probably again involve a phase separation. Experimental evidence for a second phase separation in the overdoped regime is summarized in Ref.¹³, Section XI.F. This does not preclude the possibility that there is a small but finite range of doping near the optimal in which a single phase solution is stable. Interestingly, heat capacity measurements in LSCO⁶⁴ find that the gap closes to a single VHS peak at the Fermi level (see Fig. 21 of Ref.¹³) in the overdoped range, $x=0.27$. For larger overdopings, this peak remains at the Fermi level, but decreases in intensity (as might be expected in the presence of a phase separation). This suggests an even stronger pinning of the Fermi level to the VHS than expected theoretically. Note from Fig. 6 that in the overdoped regime, the CDW undergoes a quantum phase transition, $T_{CDW} \rightarrow 0$. The possible role of such a QCP on superconductivity has been discussed recently⁷⁶. However, this could be obscured by a second phase separation in the overdoped regime.

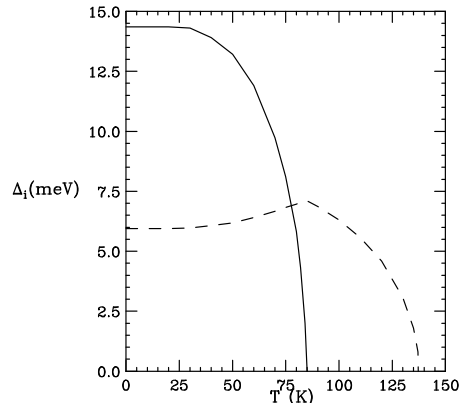


FIG. 20. Temperature dependences of the pseudogap (dashed line) and the superconducting gap (solid line) in the one-band model.

There have been a number of alternative interpretations of the pseudogap. The strictly magnetic models⁷⁷ have difficulty explaining why a gap is also seen in the charge spectrum, including photoemission and heat capacity. Other models suggest that it is associated with local pair formation, as a precursor effect to superconductivity⁷⁸. However, in overdoped materials, the pseudogap transition lies at a lower temperature than

the superconducting transition⁷⁹. Moreover, these models do not explain the frequent association of the pseudogap with structural anomalies, Ref.¹³, Section IX.A,B. Perhaps the clearest example is in $\text{YBa}_2\text{Cu}_4\text{O}_8$. Even when stoichiometric, this material is underdoped, behaving in many ways like $\text{YBa}_2\text{Cu}_3\text{O}_{6.6}$, with a pseudogap onset near 150K. When some of the Y is replaced by Ca, a transition to a long-range structurally ordered phase is found at nearly the same transition temperature⁸⁰. Moreover, the theory predicts that, in the doping range where both phases coexist, the onset of superconductivity leads to a softening of the pseudogap, Fig. 20. This can explain a number of observations of lattice anomalies at T_c , Ref.¹³, Section IX.C.

While the present model provides an impressive picture for pseudogap formation in the presence of dynamic stripes, it must be recalled that a number of intermediate steps need to be filled in. These include: (1) determination of the factors which stabilize the magnetic insulating phase at half filling; (2) self consistent calculation of the band parameters in a static striped phase; and (3) incorporation of dynamical fluctuations into the calculation. In addition, a more detailed analysis of just which phonon modes are coupled is necessary, to see how both the smaller DW gap and the superconducting gap can be d-wave. Despite these limitations, it is clear that the present calculations have the ability to explain both the stripes and the pseudogap within a common theoretical framework.

¹ P. Coleman, Phys. Rev. **B28**, 5255 (1983); N. Read and D. Newns, Sol. St. Commun. **52**, 933 (1984); A. Auerbach and K. Levin, Phys. Rev. Lett. **57**, 877 (1987).

² G. Kotliar, P.A. Lee, and N. Read, Physica **C153-155**, 538 (1988).

³ C.A.R. Sa de Melo and S. Doniach, Phys. Rev. **B41**, 6633 (1990).

⁴ R.S. Markiewicz, J. Phys. Cond. Matt. **2**, 665 (1990).

⁵ M. Grilli, G. Kotliar, and A.J. Millis, Phys. Rev. **B42**, 329 (1990).

⁶ D.M. Newns, P.C. Pattnaik, and C.C. Tsuei, Phys. Rev. **B43**, 3075 (1991).

⁷ E. Dagotto, A. Nazarenko, and M. Boninsegni, Phys. Rev. Lett. **73**, 728 (1994); N. Bulut, D.J. Scalapino, and S.R. White, Phys. Rev. Lett. **73**, 748 (1994), and Phys. Rev. **B50**, 7215 (1994).

⁸ C. Castellani, G. Kotliar, R. Raimondi, M. Grilli, Z. Wang, and M. Rozenberg, Phys. Rev. Lett. **69**, 2009 (1992).

⁹ R.S. Markiewicz, Physica **C228**, 227 (1994).

¹⁰ H. Endres, W. Hanke, H.G. Evertz, and F.F. Assaad, unpublished (cond-mat/9609219).

¹¹ G. Dopf, A. Muramatsu, and W. Hanke, Phys. Rev. **B41**, 9264 (1990).

¹² R.T. Scalettar, D.J. Scalapino, R.L. Sugar, and S.R. White,

Phys. Rev. **B44**, 770 (1991).

¹³ R.S. Markiewicz, J. Phys. Chem. Sol., to be published.

¹⁴ P.H. Dickinson and S. Doniach, Phys. Rev. **B47**, 11447 (1993).

¹⁵ S. Caprara and M. Grilli, Phys. Rev. **B49**, 6971 (1994).

¹⁶ S. Caprara, C. DiCastro and M. Grilli, Phys. Rev. **B51**, 9286 (1995).

¹⁷ R.S. Markiewicz, unpublished, and presented at the 'Stripes' Conference, Ref.^{38c}.

¹⁸ Q. Si and K. Levin, Phys. Rev. **B44**, 4727 (1991).

¹⁹ Q. Si and G. Kotliar, Phys. Rev. **B48**, 13881 (1993).

²⁰ P. Monthoux and D. Pines, Phys. Rev. **B47**, 6069 (1993).

²¹ K. Dichtel, J. Fritzenkötter, and J. Carstensen, in Ref.^{38b}, p. 365.

²² D.J. Golosov, M.L. Horbach, and A.E. Ruckenstein, J. Supercond. **8**, 659 (1995).

²³ J. González, F. Guinea, and M.A.H. Vozmediano, unpublished (cond-mat/9502095 and /9602033).

²⁴ P. Majumdar and H.R. Krishnamurthy, unpublished (cond-mat/9604057).

²⁵ R.S. Markiewicz, Physica **C193**, 323 (1992).

²⁶ R.S. Markiewicz, Phys. Rev. Lett. **73**, 1310 (1994).

²⁷ G. Kotliar, Phys. Rev. **B37**, 3664 (1988); I. Affleck and J.B. Marston, Phys. Rev. **B37**, 3774 (1988).

²⁸ C.A. Balseiro and L.M. Falicov, Phys. Rev. **B20**, 4457 (1979).

²⁹ P.B. Visscher, Phys. Rev. **B10**, 943 (1974).

³⁰ E.L. Nagaev, "Physics of Magnetic Semiconductors" (Moscow, Mir, 1983).

³¹ V. Hizhnyakov and E. Sigmund, Physica **C156**, 655 (1988).

³² V.J. Emery, S.A. Kivelson, and H.Q. Lin, Phys. Rev. Lett. **64**, 475 (1990).

³³ C. Au, B.H. Zhao, and H.T. Nieh, Phys. Rev. Lett., to be published (cond-mat/9602054); G. Su, Phys. Rev. **B54**, 8281 (1996).

³⁴ E. Dagotto, Rev. Mod. Phys. **66**, 763 (1994).

³⁵ R. Raimondi, C. Castellani, M. Grilli, Y. Bang, and G. Kotliar, Phys. Rev. **B47**, 3331 (1993).

³⁶ E. Ercolessi, P. Pieri, and M. Roncaglia, unpublished (cond-mat/9610172).

³⁷ C.S. Hellberg and E. Manousakis, unpublished (cond-mat/9611195).

³⁸ (a) "Phase Separation in Cuprate Superconductors", ed. by K.A. Müller and G. Benedek, (World, Singapore, 1992);

(b) "Phase Separation in Cuprate Superconductors", ed. by E. Sigmund and K.A. Müller, (Springer, Berlin, 1994).

(c) First Int. Conf. on Stripes, Lattice Instabilities, and High T_c Superconductivity, Rome, Dec. 8-12, 1996, to be published, J. Supercond.

³⁹ V.J. Emery and S.A. Kivelson, Physica **C209**, 597 (1993).

⁴⁰ R.S. Markiewicz, Int. J. Mod. Phys. **B5**, 2037 (1991).

⁴¹ W. Jiang, S.N. Mao, X.X. Xi, X. Jiang, J.-L. Peng, T. Venkatesan, C.J. Lobb, and R.L. Greene, Phys. Rev. Lett. **73**, 1291 (1994).

⁴² S.J.L. Billinge and T. Egami, Phys. Rev. **B47**, 14386 (1993).

⁴³ J.D. Jorgensen, B. Dabrowski, S. Pei, D.G. Hinks, L. Soderholm, B. Morosin, J.E. Schirber, E.L. Venturini, and D.S. Ginley, Phys. Rev. **B38**, 11337 (1988); M.S. Hundley, J.D. Thompson, S.-W. Cheong, Z. Fisk, and J.E. Schirber,

Phys. Rev. B**41**, 4062 (1990); P.C. Hammel, A.P. Reyes, Z. Fisk, M. Takigawa, J.D. Thompson, R.H. Heffner, S.-W. Cheong, and J.E. Schirber, Phys. Rev. B**42**, 6781 (1990).

⁴⁴ J.M. Tranquada, B.J. Sternlieb, J.D. Axe, Y. Nakamura, and S. Uchida, *Nature* **375**, 561 (1995).

⁴⁵ J.M. Tranquada, J.D. Axe, N. Ichikawa, A.R. Moodenbaugh, Y. Nakamura, and S. Uchida, unpublished (cond-mat/9608048).

⁴⁶ F. Basco, H. Kohno, H. Fukuyama, and G. Baskaran, unpublished (cond-mat/9608122).

⁴⁷ J.B. Goodenough and J.-S. Zhou, Phys. Rev. B**42**, 4276 (1990); J.B. Goodenough, *Supercond. Sci. Technol.* **3**, 26 (1990).

⁴⁸ L. Pietronero and S. Strässler, in "Physics of Intercalation Compounds", ed. by L. Pietronero and E. Tosatti, (Springer, Berlin, 1981), p. 23.

⁴⁹ F.C. Zhang and P. Prelovsek, Phys. Rev. B**37**, 1569 (1988).

⁵⁰ S. Tang and J.E. Hirsch, Phys. Rev. B**37**, 9546 (1988).

⁵¹ E. Manousakis, Rev. Mod. Phys. **63**, 1 (1991).

⁵² R.S. Markiewicz, Physica C**255**, 211 (1995).

⁵³ A.A. Abrikosov, J.C. Campuzano, K. Gofron, Physica C**214**, 73 (1993); K. Gofron, J.C. Campuzano, A.A. Abrikosov, M. Lindroos, A. Bansil, H. Ding, D. Koelling, and B. Dabrowski, Phys. Rev. Lett. **73**, 3302 (1994).

⁵⁴ D.S. Marshall, D.S. Dessau, A.G. Loeser, C.-H. Park, A.Y. Matsuura, J.N. Eckstein, I. Bozovic, P. Fournier, A. Kapitulnik, W.E. Spicer, and Z.-X. Shen, Phys. Rev. Lett. **76**, 4841 (1996).

⁵⁵ B.O. Wells, Z.X. Shen, A. Matsuura, D.M. King, M.A. Kastner, M. Greven, and R.J. Birgeneau, Phys. Rev. Lett. **74**, 964 (1995).

⁵⁶ E. Dagotto, A. Nazarenko and A. Moreo, Phys. Rev. Lett. **74**, 310 (1995).

⁵⁷ A. Nazarenko, K.J.E. Vos, S. Haas, E. Dagotto, and R.J. Gooding, J. Supercond. **8**, 671 (1995).

⁵⁸ R.B. Laughlin, J. Phys. Chem. Sol. **56**, 1627 (1995).

⁵⁹ X.-G. Wen and P.A. Lee, Phys. Rev. Lett. **76**, 503 (1996).

⁶⁰ U. Trapper, D. Ihle, and H. Fehske, Phys. Rev. B**52**, 11553 (1995).

⁶¹ A.G. Loeser, Z.-X. Shen, and D.S. Dessau, Physica C**263**, 208 (1996); A.G. Loeser, Z.-X. Shen, D.S. Dessau, D.S. Marshall, C.H. Park, P. Fournier, and A. Kapitulnik, *Science* **273**, 325 (1996).

⁶² H. Ding, T. Yokoya, J.C. Campuzano, T. Takahashi, M. Randeria, M.R. Norman, T. Mochiku, K. Kadowaki, and J. Giapintzakis, *Nature* **382**, 51 (1996).

⁶³ J.C. Campuzano, presented at the 'Stripes' Conference, Ref.³⁸c.

⁶⁴ J.W. Loram, J.R. Cooper, K.A. Mirza, N. Athanasopoulou, and W.Y. Liang, submitted to Phys. Rev. B.

⁶⁵ J.W. Loram, K.A. Mirza, J.R. Cooper, N.A. Athanasopoulou, and W.Y. Liang, presented at the 10th Anniv. HTS Workshop, Houston, TX, Mar. 12-16, 1996.

⁶⁶ R. Liu, B.W. Veal, A.P. Paulikas, J.W. Downey, H. Shi, C.G. Olson, C. Gu, A.J. Arko, and J.J. Joyce, Phys. Rev. B**45**, 5614 (1992); R. Liu, B.W. Veal, A.P. Paulikas, J.W. Downey, P.J. Kostic, S. Fleshler, U. Welp, C.G. Olson, X. Wu, A.J. Arko, and J.J. Joyce, Phys. Rev. B**46**, 11056 (1992).

⁶⁷ R. Liu, B.W. Veal, C. Gu, A.P. Paulikas, P. Kostic, and C.G. Olson, Phys. Rev. B**52**, 553 (1995).

⁶⁸ R.S. Markiewicz, Physica C**207**, 281 (1993).

⁶⁹ R.J. Elliott, J.A. Krumhansl, and P.L. Leath, Rev. Mod. Phys. **46**, 465 (1974).

⁷⁰ H. Kajueter, G. Kotliar, D.D. Sarma, and S.R. Barman, unpublished (cond-mat/9609259); D.D. Sarma, S.R. Barman, H. Kajueter, and G. Kotliar, unpublished (cond-mat/9608021)

⁷¹ A. Fujimori, I. Hase, H. Namatame, Y. Fujishima, Y. Tokura, H. Eisaki, S. Uchida, K. Takegahara, and F.M.F. deGroot, Phys. Rev. Lett. **69**, 1796 (1992); A. Fujimori, I. Hase, Y. Tokura, M. Abbe, F.M.F. deGroot, J.C. Fuggle, H. Eisaki, and S. Uchida, Physica B**186-188**, 981 (1993); I.H. Inoue, I. Hase, Y. Aiura, A. Fujimori, Y. Haruyama, T. Maruyama, and Y. Nishihara, Phys. Rev. Lett. **74**, 2539 (1995).

⁷² S.R. White and D.J. Scalapino, unpublished (cond-mat/9610104).

⁷³ J.W. Loram, K.A. Mirza, J.R. Cooper, and W.Y. Liang, Phys. Rev. Lett. **71**, 1740 (1993).

⁷⁴ J.M. Harris, Z.-X. Shen, P.J. White, D.S. Marshall, M.C. Schabel, J.N. Eckstein, and I. Bozovic, Phys. Rev. B**54**, 15665 (1996).

⁷⁵ P. Dai, M. Yethiraj, H.A. Mook, T.B. Lindemer, and F. Doğan, Phys. Rev. Lett. **77**, 5425 (1996); H.F. Fong, B. Keimer, D.L. Milius, and I.A. Aksay, unpublished (cond-mat/9612110).

⁷⁶ A. Perali, C. Castellani, C. Di Castro, and M. Grilli, Phys. Rev. B**54**, 16216 (1996).

⁷⁷ Y. Suzumura, Y. Hasegawa, and H. Fukuyama, J. Phys. Soc. Jpn. **57**, 401 (1988); N. Nagaosa and P.A. Lee, Phys. Rev. B**45**, 966 (1992); M.U. Ubbens and P.A. Lee, Phys. Rev. B**49**, 6853 (1994).

⁷⁸ C.A.R. Sa de Melo, et al., Phys. Rev. Lett. **71**, 3202 (1993); V.J. Emery and S.A. Kivelson, *Nature* **274**, 434 (1995); J. Maly, K. Levin, and D.Z. Liu, Phys. Rev. B**54**, 15657 (1996).

⁷⁹ J.L. Tallon, J.R. Cooper, P.S.I.P.N. de Silva, G.V.M. Williams, and J.W. Loram, Phys. Rev. Lett. **75**, 4114 (1995); P.J. White, Z.-X. Shen, C. Kim, J.M. Harris, A.G. Loeser, P. Fournier, and A. Kapitulnik, Phys. Rev. B**54**, 15669 (1996).

⁸⁰ W. Ting, O.-M. Nes, T. Suzuki, M.G. Karkut, K. Fossheim, Y. Yaegashi, H. Yamauchi, and S. Tanaka, Phys. Rev. B**48**, 607 (1993); W. Ting and K. Fossheim, *J. Alloys & Cpd.* **211-212**, 260 (1994).